Detecting and Adapting to Parameter Changes for Reduced Models of Dynamic Data-driven Application Systems

Citation: Peherstorfer, Benjamin, and Karen Willcox. "Detecting and Adapting to Parameter Changes for Reduced Models of Dynamic Data-Driven Application Systems." Procedia Computer Science 51 (2015): 2553–2562.

As Published: http://dx.doi.org/10.1016/j.procs.2015.05.363

Publisher: Elsevier

Persistent URL: http://hdl.handle.net/1721.1/106324

Version: Final published version: final published article, as it appeared in a journal, conference proceedings, or other formally published context

Procedia Computer Science

Volume 51, 2015, Pages 2553–2562

ICCS 2015 International Conference On Computational Science

Detecting and adapting to parameter changes for reduced models of dynamic data-driven application systems

Benjamin Peherstorfer[1] and Karen Willcox[1]

Department of Aeronautics & Astronautics, MIT, 77 Massachusetts Avenue, Cambridge, MA 02139
pehersto@mit.edu

Abstract

We consider the task of dynamic capability estimation for an unmanned aerial vehicle, which is needed to provide the vehicle with the ability to dynamically and autonomously sense, plan, and act in real time. Our dynamic data-driven application systems framework employs reduced models to achieve rapid evaluation runtimes. Our reduced models must also adapt to underlying dynamic system changes, such as changes due to structural damage or degradation of the system. Our dynamic reduced models take into account changes in the underlying system by directly learning from the data provided by sensors, without requiring access to the original high-fidelity model. We present here an adaptivity indicator that detects a change in the underlying system and so allows the initiation of the dynamic reduced modeling adaptation if necessary. The adaptivity indicator monitors the error of the dynamic reduced model by comparing model predictions with sensor data, and signals a change if the error exceeds a given threshold. The indicator is demonstrated on a deflection model of a damaged plate in bending. Local damage of the plate is modeled by a change in the thickness of the plate. The numerical results show that in this example the adaptivity indicator detects all changes in the thickness and correctly initiates the adaptation of the reduced model.

Keywords: dynamic data-driven application systems, dynamic reduced models, model reduction

1 Introduction

Modern aerospace vehicles are becoming increasingly independent of human interaction in-flight. Technologies range from *unmanned*—vehicles that do not require a human operator in an airborne position but may require real-time interaction remotely via a pilot on the ground—to *autonomous*—vehicles that are able to make in-flight mission-critical decisions and react to stimuli in the environment. A critical method for furthering autonomy is to produce *self-aware* systems: not only can these systems plan and operate independently of human operators, they are also able to quantify the state of their available internal resources and maintain knowledge of their current health beyond their initial baseline performance [3, 8]. In this way, the system

Selection and peer-review under responsibility of the Scientific Programme Committee of ICCS 2015

doi:10.1016/j.procs.2015.05.363

mimics behavior of a biological organism—it can act aggressively when it is healthy and in favorable conditions, and can become more conservative as it ages and degrades.

There are several challenges associated with enabling a self-aware vehicle. Among them is the task of dynamic capability estimation, needed to provide the vehicle with the ability to dynamically and autonomously observe, orient, decide, and act in real time. In our dynamic data-driven application systems (DDDAS) framework, models and computational methods invoked in the online decision-making phase have to meet two particular requirements. First, a decision has to be made in a time-constrained environment and thus the model evaluation runtime must be short. Second, the underlying dynamic system changes (e.g., due to structural damage or degradation) which in turn requires the model to adapt to these changes. The runtime constraints can be addressed by employing model reduction; however, classical model reduction follows a static approach where the reduced model is built once in the offline phase and then stays fixed during the computations in the online phase. Thus, if the underlying system changes, the reduced model either becomes invalid or has to be rebuilt from scratch. Rebuilding the reduced model requires access to, and often evaluations of, the computationally expensive high-fidelity model and so becomes quickly computationally infeasible if only limited computing resources are available.

Our recent work has proposed a dynamic reduced modeling methodology that breaks with this rigid splitting into offline and online phases [12]. Our dynamic reduced models take into account changes in the underlying system by directly learning from data, without requiring access to the high-fidelity model. The data are provided by, e.g., sensors. Our work differs from other recent approaches in reduced model adaptation (e.g., [1, 11, 10, 15, 5, 6]) in that we do not anticipate offline how the high-fidelity, and thus the reduced model changes during the online phase, and that we incorporate new information in the form of sensor data for the update.

We model system changes with latent parameters and inputs to the system with observable parameters. The latent parameters are prescribed by external influences and cannot be controlled. Note that latent parameters here do not necessarily capture all possible external influences onto the system. The values of the latent parameters are unknown, except for initial latent parameters. If the latent parameters change, the reduced model becomes obsolete and has to be adapted. In the following, we extend the adaptation methodology [12] with an adaptivity indicator that detects when the latent parameters have changed and then informs the dynamic reduced modeling adaptation. The adaptivity indicator is based on monitoring the error of the dynamic reduced model by comparing model predictions with the sensor data. If the error exceeds a certain threshold then a change in the latent parameters is signaled. Note that our adaptivity indicator only detects a change in the latent parameters and does not infer the actual value of the latent parameters.

2 Systems with observable and latent parameters

We consider a model that is based on a parametrized partial differential equation (PDE). The high-fidelity model stems from the discretization of the PDE and is the system of equations

$$\boldsymbol{A}_{\boldsymbol{\eta}}(\boldsymbol{\mu})\boldsymbol{y}_{\boldsymbol{\eta}}(\boldsymbol{\mu}) = \boldsymbol{f}(\boldsymbol{\mu})\,, \tag{1}$$

with $\mathcal{N} \in \mathbb{N}$ degrees of freedom, the observable parameter $\boldsymbol{\mu} = [\mu_1, \ldots, \mu_d]^T \in \mathcal{D} \subset \mathbb{R}^d, d \in \mathbb{N}$, and the latent parameter $\boldsymbol{\eta} = [\eta_1, \ldots, \eta_{d'}]^T \in \mathcal{E} \subset \mathbb{R}^{d'}, d' \in \mathbb{N}$. Note that $\boldsymbol{\mu}$ and $\boldsymbol{\eta}$ are vectors and therefore the system (1) can have multiple observable and latent parameters although we

refer in the following to the vectors $\boldsymbol{\mu}$ and $\boldsymbol{\eta}$ as observable and latent parameter (singular). The linear operator $\boldsymbol{A}_{\boldsymbol{\eta}}(\boldsymbol{\mu}) \in \mathbb{R}^{\mathcal{N}\times\mathcal{N}}$ and the state vector $\boldsymbol{y}_{\boldsymbol{\eta}}(\boldsymbol{\mu}) \in \mathbb{R}^{\mathcal{N}}$ depend on the observable and the latent parameter. The right-hand side $\boldsymbol{f}(\boldsymbol{\mu}) \in \mathbb{R}^{\mathcal{N}}$ depends on the observable parameter only. The initial state of the system is described by the initial latent parameter $\boldsymbol{\eta}_0 \in \mathcal{E}$. Note that the value of the initial latent parameter is known.

We construct a reduced model of the high-fidelity model (1) with respect to the initial latent parameter $\boldsymbol{\eta}_0$. First, a reduced basis with proper orthogonal decomposition (POD) [2, 13] is constructed, and then a reduced system of (1) is derived with Galerkin projection.

We select $M \in \mathbb{N}$ observable parameters $\boldsymbol{\mu}_1, \ldots, \boldsymbol{\mu}_M \in \mathcal{D}$, following a suitable sampling strategy [14, 9, 4]. The snapshots

$$\boldsymbol{y}_{\boldsymbol{\eta}_0}(\boldsymbol{\mu}_1), \ldots, \boldsymbol{y}_{\boldsymbol{\eta}_0}(\boldsymbol{\mu}_M) \in \mathbb{R}^{\mathcal{N}} \tag{2}$$

are the solutions of the high-fidelity model (1) for the selected observable parameters $\boldsymbol{\mu}_1, \ldots, \boldsymbol{\mu}_M \in \mathcal{D}$ and the initial latent parameter $\boldsymbol{\eta}_0$. POD generates $n \in \mathbb{N}, n \ll \mathcal{N}$ basis vectors $\boldsymbol{v}_1, \ldots, \boldsymbol{v}_n \in \mathbb{R}^{\mathcal{N}}$ of the snapshots (2), which we put as columns in the matrix $\boldsymbol{V}_0 \in \mathbb{R}^{\mathcal{N}\times n}$. The subscript 0 of $\boldsymbol{V}_0$ indicates that the POD basis vectors in $\boldsymbol{V}_0$ depend on the latent parameter $\boldsymbol{\eta}_0$. The reduced model of the high-fidelity model (1) is given by the system of equations

$$\tilde{\boldsymbol{A}}_0(\boldsymbol{\mu})\tilde{\boldsymbol{y}}_0(\boldsymbol{\mu}) = \tilde{\boldsymbol{f}}_0(\boldsymbol{\mu})\,, \tag{3}$$

with the reduced operator $\tilde{\boldsymbol{A}}_0(\boldsymbol{\mu}) = \boldsymbol{V}_0^T \boldsymbol{A}_{\boldsymbol{\eta}_0}(\boldsymbol{\mu})\boldsymbol{V}_0 \in \mathbb{R}^{n\times n}$, the reduced state vector $\tilde{\boldsymbol{y}}_0(\boldsymbol{\mu}) \in \mathbb{R}^n$, and the reduced right-hand side $\tilde{\boldsymbol{f}}_0(\boldsymbol{\mu}) = \boldsymbol{V}_0^T \boldsymbol{f}(\boldsymbol{\mu}) \in \mathbb{R}^n$. For details on how to efficiently compute $\tilde{\boldsymbol{A}}_0(\boldsymbol{\mu})$ for a given observable parameter $\boldsymbol{\mu}$ see [12] and the references therein. We note that the reduced right-hand side depends through the POD basis $\boldsymbol{V}_0$ on the latent parameter $\boldsymbol{\eta}_0$, whereas the right-hand side $\boldsymbol{f}$ of the high-fidelity model (1) is independent of the latent parameter. In many situations, choosing $n \ll \mathcal{N}$ leads to a reduced state vector $\tilde{\boldsymbol{y}}_0(\boldsymbol{\mu})$ such that $\boldsymbol{V}_0\tilde{\boldsymbol{y}}_0(\boldsymbol{\mu})$ approximates $\boldsymbol{y}_{\boldsymbol{\eta}_0}(\boldsymbol{\mu})$ well. Since $n \ll \mathcal{N}$, the reduced system (3) is often computationally faster to solve than (1).

3 Dynamic reduced models

We consider the following problem setup of dynamic reduced models [12]. In the offline phase, the dynamic reduced model (3) is built for the initial latent parameter $\boldsymbol{\eta}_0$ as described in Section 2. In the online phase, the reduced model is evaluated at observable parameters of interest and adapted to system changes. The online phase consists of $M' \in \mathbb{N}$ steps, which we denote with $h = 1, \ldots, M'$. At each step, a sensor sample $\hat{\boldsymbol{y}}_{\boldsymbol{\eta}_h}(\boldsymbol{\mu}_{M+h}) \in \mathbb{R}^{\mathcal{N}}$ is received. The latent parameter $\boldsymbol{\eta}_h \in \mathcal{E}$ is unknown. The observable parameter $\boldsymbol{\mu}_{M+h} \in \mathcal{D}$ is known but cannot be influenced and changed. The sensor sample $\hat{\boldsymbol{y}}_{\boldsymbol{\eta}_h}(\boldsymbol{\mu}_{M+h})$ is a measurement of the state vector $\boldsymbol{y}_{\boldsymbol{\eta}_h}(\boldsymbol{\mu}_{M+h})$ of the high-fidelity model (1), where the difference $\boldsymbol{y}_{\boldsymbol{\eta}_h}(\boldsymbol{\mu}_{M+h}) - \hat{\boldsymbol{y}}_{\boldsymbol{\eta}_h}(\boldsymbol{\mu}_{M+h})$ is measurement noise and high-fidelity model error. If the latent parameter changes from step $h-1$ to h, i.e., if $\boldsymbol{\eta}_{h-1} \neq \boldsymbol{\eta}_h$, then the dynamic reduced modeling adaptation needs to be initiated. Adapting the dynamic reduced model means adapting the POD basis, the reduced operator, and the reduced right-hand side.

The dynamic reduced modeling adaptation was introduced in [12]. At step $h = 1$, the sensor sample $\hat{\boldsymbol{y}}_{\boldsymbol{\eta}_1}(\boldsymbol{\mu}_{M+1}) \in \mathbb{R}^{\mathcal{N}}$ is received and the pointer $k_1 \in \mathbb{N}$ is initialized as $k_1 = 1$. The sensor sample is put as a column in the sensor window

$$\boldsymbol{S}_1 = [\hat{\boldsymbol{y}}_{\boldsymbol{\eta}_1}(\boldsymbol{\mu}_{M+1})] \in \mathbb{R}^{\mathcal{N}\times 1}\,.$$

Algorithm 1 Dynamic reduced modeling adaptation

procedure ADAPTROM($\boldsymbol{S}_{h-1}$, k_{h-1}, $\boldsymbol{V}_{h-1}$, $\tilde{\boldsymbol{A}}_{h-1}$, $\tilde{\boldsymbol{f}}_{h-1}$)
  Receive new sensor sample $\hat{\boldsymbol{y}}_{\boldsymbol{\eta}_h}(\boldsymbol{\mu}_{M+h}) \in \mathbb{R}^{\mathcal{N}}$
  Extend sensor window to

$$\boldsymbol{S}_h = [\hat{\boldsymbol{y}}_{\boldsymbol{\eta}_1}(\boldsymbol{\mu}_{M+1}), \ldots, \hat{\boldsymbol{y}}_{\boldsymbol{\eta}_h}(\boldsymbol{\mu}_{M+h})] \in \mathbb{R}^{\mathcal{N} \times h}$$

  if latent parameter changed, i.e., $\boldsymbol{\eta}_{h-1} \neq \boldsymbol{\eta}_h$ **then**
    Set pointer $k_h = h$
  else
    Set pointer $k_h = k_{h-1}$
  end if
  Adapt POD basis to $\boldsymbol{V}_h$ using sensor samples

$$\hat{\boldsymbol{y}}_{\boldsymbol{\eta}_{k_h}}(\boldsymbol{\mu}_{M+k_h}), \ldots, \hat{\boldsymbol{y}}_{\boldsymbol{\eta}_h}(\boldsymbol{\mu}_{M+h}) \tag{4}$$

  Adapt reduced operator to $\tilde{\boldsymbol{A}}_h$ using sensor samples (4)
  Adapt right-hand side to $\tilde{\boldsymbol{f}}_h$ using sensor samples (4)
  return $\boldsymbol{S}_h, k_h, \boldsymbol{V}_h, \tilde{\boldsymbol{A}}_h, \tilde{\boldsymbol{f}}_h$
end procedure

At step $h = 1$, the adaptation updates the reduced model with the sensor sample in the sensor window $\boldsymbol{S}_1$. The POD basis $\boldsymbol{V}_0$ is adapted to $\boldsymbol{V}_1$, the reduced operator $\tilde{\boldsymbol{A}}_0$ to $\tilde{\boldsymbol{A}}_1$, and the reduced right-hand side $\tilde{\boldsymbol{f}}_0$ to $\tilde{\boldsymbol{f}}_1$. We refer to [12] for details on the adaptation procedure. At step $h = 1$, there is only one sensor sample and thus the pointer k_1 is ignored. In the second step $h = 2$, the sensor sample $\hat{\boldsymbol{y}}_{\boldsymbol{\eta}_2}(\boldsymbol{\mu}_{M+2})$ is received and the sensor window is extended to

$$\boldsymbol{S}_2 = [\hat{\boldsymbol{y}}_{\boldsymbol{\eta}_1}(\boldsymbol{\mu}_{M+1}), \hat{\boldsymbol{y}}_{\boldsymbol{\eta}_2}(\boldsymbol{\mu}_{M+2})] \in \mathbb{R}^{\mathcal{N} \times 2}\,.$$

If $\boldsymbol{\eta}_1 = \boldsymbol{\eta}_2$, both sensor samples in $\boldsymbol{S}_2$ correspond to the same latent parameter. Therefore, both sensor samples can be used for the adaptation. The pointer is set to $k_2 = k_1 = 1$, and the sensor samples $\hat{\boldsymbol{y}}_{\boldsymbol{\eta}_1}(\boldsymbol{\mu}_{M+1}), \hat{\boldsymbol{y}}_{\boldsymbol{\eta}_2}(\boldsymbol{\mu}_{M+2})$ are used to adapt the POD basis to $\boldsymbol{V}_2$, the reduced operator to $\tilde{\boldsymbol{A}}_2$, and the reduced right-hand side to $\tilde{\boldsymbol{f}}_2$. If $\boldsymbol{\eta}_1 \neq \boldsymbol{\eta}_2$, the latent parameter has changed. All sensor samples in the sensor window received before step $h = 2$ are ignored. Therefore, the pointer is set to $k_2 = h = 2$, and only the sensor sample $\hat{\boldsymbol{y}}_{\boldsymbol{\eta}_2}(\boldsymbol{\mu}_{M+2})$ is used for the adaptation to the latent parameter $\boldsymbol{\eta}_2$. This process is continued. At step h, sensor sample $\hat{\boldsymbol{y}}_{\boldsymbol{\eta}_h}(\boldsymbol{\mu}_{M+h})$ is received. If $\boldsymbol{\eta}_{h-1} = \boldsymbol{\eta}_h$, the pointer is set to $k_h = k_{h-1}$. If $\boldsymbol{\eta}_{h-1} \neq \boldsymbol{\eta}_h$, the pointer is set to $k_h = h$. Then, the sensor samples $\hat{\boldsymbol{y}}_{\boldsymbol{\eta}_{k_h}}(\boldsymbol{\mu}_{M+k_h}), \ldots, \hat{\boldsymbol{y}}_{\boldsymbol{\eta}_h}(\boldsymbol{\mu}_{M+h})$ are used for the adaptation of the POD basis $\boldsymbol{V}_{h-1}$ to $\boldsymbol{V}_h$, the reduced operator $\tilde{\boldsymbol{A}}_{h-1}$ to $\tilde{\boldsymbol{A}}_h$, and the reduced right-hand side $\tilde{\boldsymbol{f}}_{h-1}$ to $\tilde{\boldsymbol{f}}_h$. The adaptation procedure is summarized in Algorithm 1.

4 Adaptivity indicator for dynamic reduced models

The dynamic reduced model procedure summarized in Algorithm 1 modifies the pointer k_h at step h depending on whether the latent parameter has changed. We emphasize that for the check if the latent parameter has changed, it is unnecessary to know the value of the latent parameter, just that it has changed. In this section, we present an adaptivity indicator that

heuristically detects if the latent parameter has changed by monitoring the error of the reduced model. The following procedure is specifically designed for dynamic reduced models.

Consider step $h-1$ with pointer k_{h-1} and sensor window

$$\boldsymbol{S}_{h-1} = [\hat{\boldsymbol{y}}_{\boldsymbol{\eta}_1}(\boldsymbol{\mu}_{M+1}), \ldots, \hat{\boldsymbol{y}}_{\boldsymbol{\eta}_{h-1}}(\boldsymbol{\mu}_{M+h-1})] \in \mathbb{R}^{\mathcal{N} \times h-1} .$$

At step h, we receive the sensor sample $\hat{\boldsymbol{y}}_{\boldsymbol{\eta}_h}(\boldsymbol{\mu}_{M+h})$. Since the observable parameters of the sensor samples are known (see the problem description in Section 3), we can evaluate the reduced model of step $h-1$ at the observable parameters $\boldsymbol{\mu}_{M+k_{h-1}}, \ldots, \boldsymbol{\mu}_{M+h} \in \mathcal{D}$ corresponding to the sensor samples

$$\hat{\boldsymbol{y}}_{\boldsymbol{\eta}_{k_{h-1}}}(\boldsymbol{\mu}_{M+k_{h-1}}), \ldots, \hat{\boldsymbol{y}}_{\boldsymbol{\eta}_h}(\boldsymbol{\mu}_{M+h}) \in \mathbb{R}^{\mathcal{N}} \tag{5}$$

that were received at the steps from k_{h-1}, when the adaptation starts, through the current step h. Evaluating the reduced model of step $h-1$ at $\boldsymbol{\mu}_{M+k_{h-1}}, \ldots, \boldsymbol{\mu}_{M+h}$ means solving the reduced system

$$\tilde{\boldsymbol{A}}_{h-1}(\boldsymbol{\mu}_{M+i})\tilde{\boldsymbol{y}}_{h-1}(\boldsymbol{\mu}_{M+i}) = \tilde{\boldsymbol{f}}_{h-1}(\boldsymbol{\mu}_{M+i}) ,$$

for $i = k_{h-1}, \ldots, h$. We obtain the reduced state vectors

$$\tilde{\boldsymbol{y}}_{h-1}(\boldsymbol{\mu}_{M+k_{h-1}}), \ldots, \tilde{\boldsymbol{y}}_{h-1}(\boldsymbol{\mu}_{M+h}) \in \mathbb{R}^n . \tag{6}$$

The average relative L_2 error of the approximate state reconstruction from the reduced state vectors (6) with respect to the sensor samples (5) is denoted as

$$a_h = \sum_{i=k_{h-1}}^{h} \frac{\|\hat{\boldsymbol{y}}_{\boldsymbol{\eta}_i}(\boldsymbol{\mu}_{M+i}) - \boldsymbol{V}_{h-1}\tilde{\boldsymbol{y}}_{h-1}(\boldsymbol{\mu}_{M+i})\|_2}{\|\hat{\boldsymbol{y}}_{\boldsymbol{\eta}_i}(\boldsymbol{\mu}_{M+i})\|_2} . \tag{7}$$

Additionally, we define the current error of the sensor sample at step h as

$$e_h = \frac{\|\hat{\boldsymbol{y}}_{\boldsymbol{\eta}_h}(\boldsymbol{\mu}_{M+h}) - \boldsymbol{V}_{h-1}\tilde{\boldsymbol{y}}_{h-1}(\boldsymbol{\mu}_{M+h})\|_2}{\|\hat{\boldsymbol{y}}_{\boldsymbol{\eta}_h}(\boldsymbol{\mu}_{M+h})\|_2} . \tag{8}$$

Let $0 < \lambda \in \mathbb{R}$ be a threshold parameter. At step h, a change in the latent parameter is signaled if

$$\lambda e_h > \frac{1}{2}|a_{k_{h-1}} + a_h| \tag{9}$$

holds. The term λe_h on the left of (9) is the relative L_2 error e_h of the reduced model of the previous step $h-1$ at the current sensor sample $\hat{\boldsymbol{y}}_{\boldsymbol{\eta}_h}(\boldsymbol{\mu}_{M+h})$, weighted with the threshold parameter λ. The term $1/2|a_{k_{h-1}} + a_h|$ on the right is the value between the error $a_{k_{h-1}}$, when the adaptation started at step k_{h-1}, and the current average error a_h. Since the dynamic reduced model is adapted at each of the previous steps, it is reasonable to expect that the average error decreased as the adaptation continued. The indicator (9) therefore signals a change if the weighted error λe_h is above of half the accuracy that has been gained by the adaptation since step k_{h-1}. The adaptivity indicator is summarized in Algorithm 2.

5 Numerical results

We demonstrate dynamic reduced models with our adaptivity indicator on a model of a plate in bending, where the latent parameter describes local damage. The high-fidelity and the reduced model are introduced in Section 5.1 and numerical results are discussed in Section 5.2.

Algorithm 2 Indicator to detect change in latent parameter

procedure DETECTCHANGE($\boldsymbol{S}_{h-1}$, $\tilde{\boldsymbol{A}}_{h-1}$, $\tilde{\boldsymbol{f}}_{h-1}$, $\hat{\boldsymbol{y}}_{\boldsymbol{\eta}_h}(\boldsymbol{\mu}_{M+h})$, k_{h-1}, λ)
  Evaluate reduced model of step $h-1$ at parameters of sensor samples received since step k_{h-1} (5)
  Compute average relative L_2 error a_h as defined in (7)
  Compute relative L_2 error e_h corresponding to current sensor sample as in (8)
  if $\lambda e_h > \frac{1}{2}|a_{k_{h-1}} + a_h|$ **then**
    return True
  else
    return False
  end if
end procedure

5.1 Plate problem

We consider a model based on the Mindlin plate theory [7] of a clamped plate. We are interested in the deflection of the plate when a load is applied. The spatial domain $\Omega = [0,1]^2 \subset \mathbb{R}^2$ is partitioned into four square subregions $\Omega_1, \ldots, \Omega_4$. In each subregion, the thickness of the plate and the load are each controlled by an observable parameter. The model therefore has the eight-dimensional observable parameter $\boldsymbol{\mu} = [\mu_1, \ldots, \mu_8]^T \in \mathcal{D} = [0.05, 0.1]^4 \times [1, 100]^4 \subset \mathbb{R}^8$, where for $i = 1, \ldots, 4$ the parameters μ_i and μ_{4+i} control the thickness and the load in subregion Ω_i, respectively. The model has the two-dimensional latent parameter $\boldsymbol{\eta} = [\eta_1, \eta_2]^T \in \mathcal{E} = [0, 0.2] \times (0, 0.05] \subset \mathbb{R}^2$ that controls the decrease of the thickness at position $\boldsymbol{z} = [0.7, 0.4]^T \in \Omega$. A decrease of the thickness at $\boldsymbol{z}$ models local damage. The thickness of the plate at $\boldsymbol{x} \in \Omega$ is given by the value of the function

$$t(\boldsymbol{x}; \boldsymbol{\mu}, \boldsymbol{\eta}) = t_0(\boldsymbol{x}; \boldsymbol{\mu}) - t_0(\boldsymbol{x}; \boldsymbol{\mu}) \eta_1 \exp\left(-\frac{1}{2\eta_2^2} \|\boldsymbol{x} - \boldsymbol{z}\|_2^2 \right), \tag{10}$$

where

$$t_0(\boldsymbol{x}; \boldsymbol{\mu}) = \begin{cases} \mu_1 & \text{if } x_1 < 0.5 \text{ and } x_2 < 0.5 \\ \mu_2 & \text{if } x_1 < 0.5 \text{ and } x_2 \geq 0.5 \\ \mu_3 & \text{if } x_1 \geq 0.5 \text{ and } x_2 < 0.5 \\ \mu_4 & \text{if } x_1 \geq 0.5 \text{ and } x_2 \geq 0.5 \end{cases} \tag{11}$$

The initial latent parameter is $\boldsymbol{\eta}_0 = [0, \epsilon]^T$, where $\epsilon > 0$ is an arbitrary scalar that has no influence on the thickness. The high-fidelity model of the plate is obtained with the finite element method as discussed in [7, 12]. The high-fidelity model has $\mathcal{N} = 19039$ degrees of freedom.

Figure 1a shows the thickness t for $[\mu_1, \mu_2, \mu_3, \mu_4]^T = [0.08, 0.06, 0.07, 0.065]^T$ and $\boldsymbol{\eta} = \boldsymbol{\eta}_0$, and Figure 1c the deflection of the plate if the load $[\mu_5, \mu_6, \mu_7, \mu_8]^T = [50, 50, 100, 50]^T$ is applied. For the same observable parameter, the thickness and the deflection are shown in Figures 1b and 1d, respectively, for latent parameter $\boldsymbol{\eta} = [0.2, 0.05]^T$.

A reduced model is constructed with POD and Galerkin projection for the initial latent parameter $\boldsymbol{\eta}_0$ as discussed in Section 2. The POD basis $\boldsymbol{V}_0$ is generated from $M = 1000$ snapshots, where the observable parameters were drawn uniformly from $\mathcal{D}$. The reduced model has $n = 50$ degrees of freedom. This is the same reduced model as used in [12].

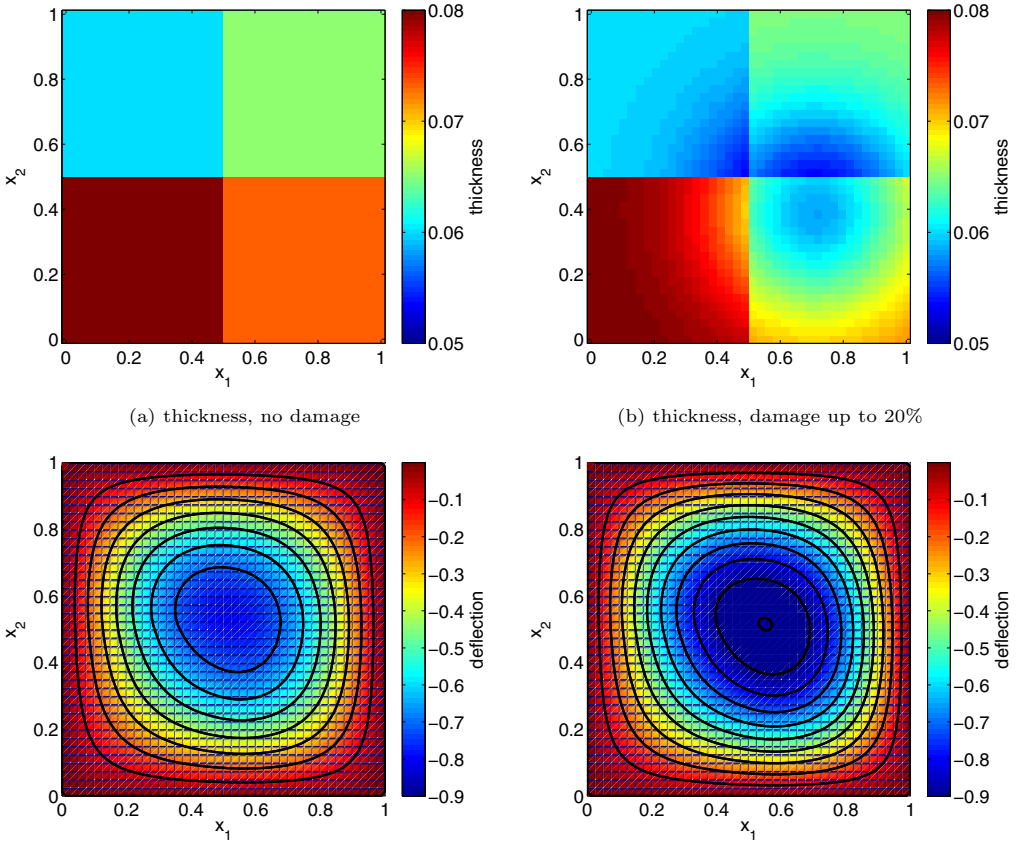

(a) thickness, no damage

(b) thickness, damage up to 20%

(c) deflection, no damage

(d) deflection, damage up to 20%

Figure 1: The plot shows the thickness without damage in (a) and with damage at $\boldsymbol{z} = [0.7, 0.4]^T \in \Omega$ in (b). The corresponding deflection of the plate is shown in (c) and (d), respectively.

5.2 Numerical experiments

We demonstrate the adaptivity indicator on the plate model. The latent parameter is changed in ten equidistant steps from $\boldsymbol{\eta}_0 = [0, \epsilon]^T$ to $[0.2, 0.05]^T$, which corresponds to a decrease of the thickness by up to 20%. After each change of the latent parameter, 600 sensor samples are read. We generate synthetic sensor samples that are the solutions of the high-fidelity model and that are not corrupted with noise. We have $M' = 10 \times 600 = 6000$ online steps $h = 1, \ldots, M'$. At each step h, the average absolute L_2 error over a test set with ten randomly chosen observable parameters is computed.

Figure 2 compares the error of the static, the dynamic, and the true reduced model: The static reduced model is built offline from snapshots with $\boldsymbol{\eta} = \boldsymbol{\eta}_0$ and is not adapted online. The dynamic reduced model is adapted online with Algorithm 1. The adaptivity indicator of Section 4 is used to check if the latent parameter has changed. The true reduced model is rebuilt from scratch from snapshots with the changed latent parameter. It is too expensive to use in a dynamic setting, but serves as a benchmark here. The threshold parameter of the

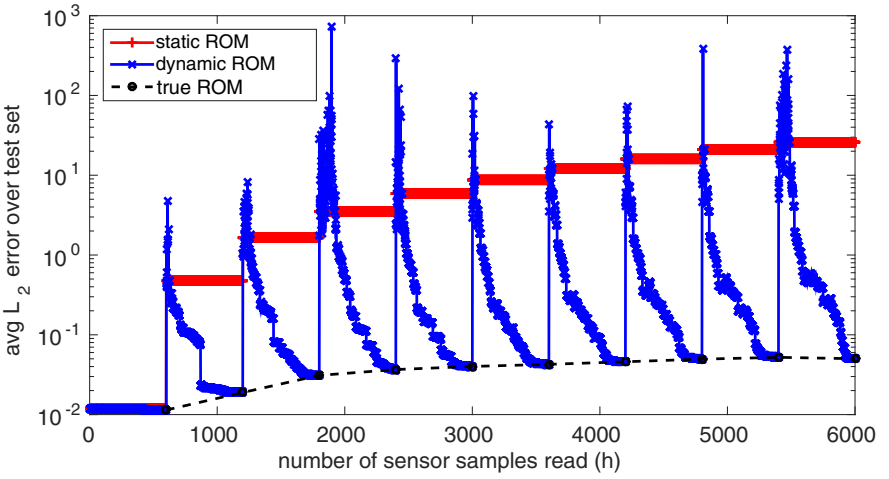

Figure 2: Setting the threshold to $\lambda = 1/8$, the adaptivity indicator detects all changes in the latent parameter in this example. The dynamic reduced model therefore can quickly adapt to changes in the underlying system and thus provides orders of magnitude more accurate predictions than the static reduced model.

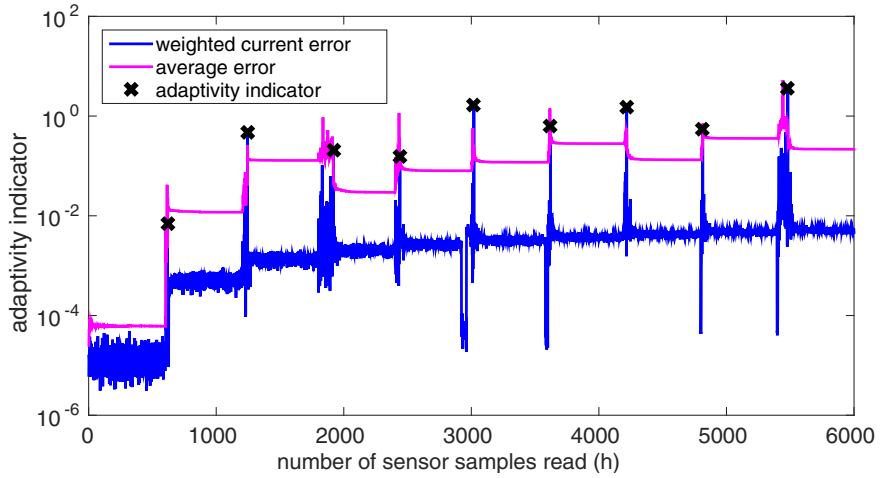

Figure 3: The plots shows the weighted current error λe_h and the average error a_h corresponding to Figure 2. The black crosses mark when the adaptivity indicator signals a change in the latent parameter.

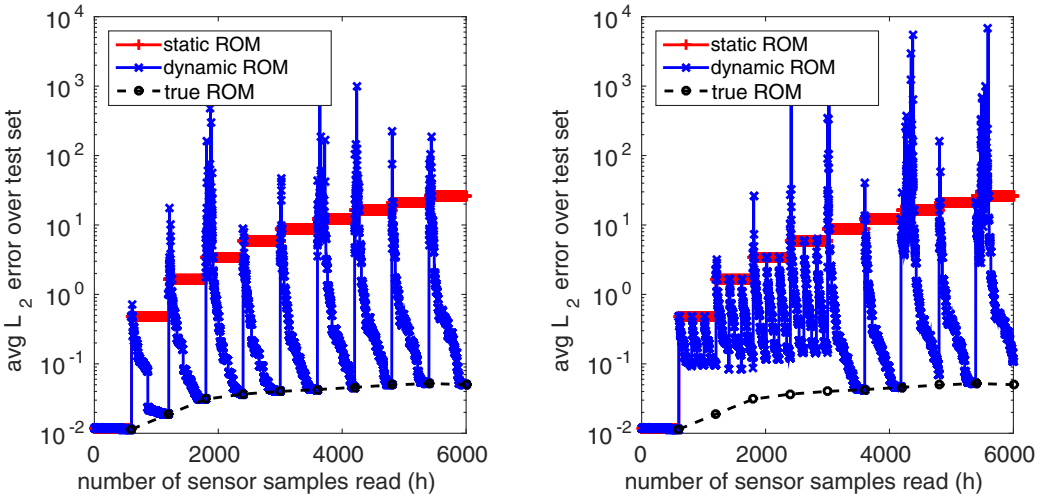

(a) threshold $\lambda = 0.25$ (b) threshold $\lambda = 1$

Figure 4: Increasing the threshold parameter λ leads to a more sensitive adaptivity indicator.

adaptivity indicator is set to $\lambda = 1/8$. The static reduced model quickly fails to provide valid approximations of the solutions of the high-fidelity model as the latent parameter, and thus the damage, changes. The dynamic reduced model adapts to the damaged plate model and achieves orders of magnitude more accurate approximations than the static reduced model. The adaptivity indicator needs a few sensor samples before it signals a change in the latent parameter. This results in high error peaks at the steps after the latent parameter has changed and before the change is detected, because the dynamic reduced modeling adaptation mixes sensor samples with different latent parameters. This mixing of sensor samples leads to invalid updates, although these are quickly corrected as more sensor data is received [12]. Figure 3 shows the weighted current error λe_h and the average error a_h corresponding to Figure 2. The current error e_h increases rapidly if the latent parameter is changed, whereas the average error a_h changes more slowly. The black crosses mark when a change in the latent parameter is detected.

In Figure 4, the effect of the threshold parameter λ is shown. If λ is set to be larger, then the adaptivity detection becomes more sensitive. If the value of λ is too large, then the indicator initiates the adaptation more often, which means that the pointer k_h is reset too early and too few sensor samples are used for the adaptation, see Algorithm 1. This can be seen in Figure 4b, where the dynamic reduced modeling adaptation suffers from too few sensor samples that are insufficient to recover the true reduced model.

6 Conclusion

We discussed model reduction in the context of DDDAS, where systems depend on inputs, modeled by an observable parameter, and external influences, modeled by a latent parameter. Dynamic reduced models adapt to changes in the latent parameter by incorporating sensor data. We presented an adaptivity indicator that signals a change in the latent parameter to initiate the adaptation. The adaptivity indicator monitors the error of the reduced model and

indicates a change in the latent parameter if the error increases relative to the average error above a threshold. In the presented numerical experiments the dynamic reduced model with the adaptivity indicator achieved orders of magnitude more accurate results than a static reduced model that was not adapted online.

Acknowledgments

This work was supported in part by AFOSR grant FA9550-11-1-0339 under the Dynamic Data-Driven Application Systems (DDDAS) Program, Program Manager Dr. Frederica Darema.

References

[1] D. Amsallem and C. Farhat. An online method for interpolating linear parametric reduced-order models. *SIAM Journal on Scientific Computing*, 33(5):2169–2198, 2011.

[2] G. Berkooz, P. Holmes, and J. Lumley. The proper orthogonal decomposition in the analysis of turbulent flows. *Annual Review of Fluid Mechanics*, 25(1):539–575, 1993.

[3] A M Brintrup, D C Ranasinghe, S Kwan, A Parlikad, K Owens, and The Boeing Company. Roadmap to Self-Serving Assets in Civil Aerospace. In *Proceedings of the 1st CIRP Industrial Product-Service Systems (IPS2) Conference*. Cranfield University, 2009.

[4] T. Bui-Thanh, K. Willcox, and O. Ghattas. Model reduction for large-scale systems with high-dimensional parametric input space. *SIAM Journal on Scientific Computing*, 30(6):3270–3288, 2008.

[5] K. Carlberg. Adaptive h-refinement for reduced-order models. *International Journal for Numerical Methods in Engineering*, 2014. accepted, available online.

[6] M. Dihlmann, M. Drohmann, and B. Haasdonk. Model reduction of parametrized evolution problems using the reduced basis method with adaptive time-partitioning. In D. Aubry, P. Dez, B. Tie, and N. Pars, editors, *Proceedings of the International Conference on Adaptive Modeling and Simulation*, pages 156–167, 2011.

[7] A. Ferreira. *MATLAB Codes for Finite Element Analysis*. Springer, 2008.

[8] D. Kordonowy and O. Toupet. Composite airframe condition-aware maneuverability and survivability for unmanned aerial vehicles. AIAA Paper 2011-1496, Infotech@Aerospace, St. Louis, Missouri, March 29–31, 2011.

[9] C. Lieberman, K. Willcox, and O. Ghattas. Parameter and state model reduction for large-scale statistical inverse problems. *SIAM Journal on Scientific Computing*, 32(5):2523–2542, 2010.

[10] Y. Maday and B. Stamm. Locally adaptive greedy approximations for anisotropic parameter reduced basis spaces. *SIAM Journal on Scientific Computing*, 35(6):A2417–A2441, 2013.

[11] B. Peherstorfer, D. Butnaru, K. Willcox, and H.-J. Bungartz. Localized discrete empirical interpolation method. *SIAM Journal on Scientific Computing*, 36(1):A168–A192, 2014.

[12] B. Peherstorfer and K. Willcox. Dynamic data-driven reduced-order models. *Computer Methods in Applied Mechanics and Engineering*, 2014. in review.

[13] L. Sirovich. Turbulence and the dynamics of coherent structures. *Quarterly of Applied Mathematics*, pages 561–571, 1987.

[14] K. Veroy and A. Patera. Certified real-time solution of the parametrized steady incompressible Navier-Stokes equations: rigorous reduced-basis a posteriori error bounds. *International Journal for Numerical Methods in Fluids*, 47(8-9):773–788, 2005.

[15] K. Washabaugh, D. Amsallem, M. Zahr, and C. Farhat. Nonlinear model reduction for CFD problems using local reduced-order bases. In *42nd AIAA Fluid Dynamics Conference and Exhibit, Fluid Dynamics and co-located Conferences, AIAA Paper 2012-2686*, pages 1–16. AIAA, 2012.